Gate voltage controlled thermoelectric figure of merit in three-dimensional topological insulator nanowires

Ning-Xuan Yang,[1] Yan-Feng Zhou,[1] Peng Lv,[1] and Qing-Feng Sun[1,2,3,*]

[1]*International Center for Quantum Materials, School of Physics, Peking University, Beijing 100871, China*

[2]*Collaborative Innovation Center of Quantum Matter, Beijing 100871, China*

[3]*CAS Center for Excellence in Topological Quantum Computation, University of Chinese Academy of Sciences, Beijing 100190, China*

(Received 28 March 2018; published 25 June 2018)

The thermoelectric properties of the surface states in three-dimensional topological insulator nanowires are studied. The Seebeck coefficients S_c and the dimensionless thermoelectrical figure of merit ZT are obtained by using the tight-binding Hamiltonian combined with the nonequilibrium Green's-function method. They are strongly dependent on the gate voltage and the longitudinal and perpendicular magnetic fields. By changing the gate voltage or magnetic fields, the values of S_c and ZT can be easily controlled. At zero magnetic field and zero gate voltage, or at large perpendicular magnetic field and nonzero gate voltage, ZT has a large value. Owing to the electron-hole symmetry, S_c is an odd function of the Fermi energy while ZT is an even function regardless of the magnetic fields. S_c and ZT show peaks when the quantized transmission coefficient jumps from one plateau to another. The highest peak appears while the Fermi energy is near the Dirac point. At zero perpendicular magnetic field and zero gate voltage, the height of the nth peak of S_C is $\frac{k_B}{e}\ln 2/(|n|+1/2)$ and $\frac{k_B}{e}\ln 2/|n|$ for the longitudinal magnetic flux $\phi_\parallel = 0$ and π, respectively. Finally, we also study the effect of disorder and find that S_c and ZT are robust against disorder. In particular, the large value of ZT can survive even at strong disorder. These characteristics (that ZT has a large value, is easily regulated, and is robust against the disorder) are very beneficial for the application of thermoelectricity.

DOI: 10.1103/PhysRevB.97.235435

I. INTRODUCTION

In recent years, the discovery of three-dimensional (3D) topological insulators (TIs) has opened up a new field for condensed-matter physics, and is also one of the most important advances in material science [1–3]. TIs have attracted wide attention because of their exotic physical properties and potential huge applications in spintronics [4–9]. TIs are characterized by the insulating bulk states and nontrivial conducting surface state, which is topologically protected by time-reversal symmetry. The time-reversal invariant disorder cannot cause the backscattering and cannot open the gap in the surface states. The surface states, which present an odd number of gapless Dirac cones, are featured by unique Dirac-like linear dispersion with spin-momentum locking helical properties [10–13]. Moreover, for a TI nanowire, a gap opened in the surface states results from the π Berry phase obtained by the 2π rotation of the spin around the nanowire [14–16]. However, by threading a magnetic flux $\phi_0/2 = h/2e$ parallel to the wire, an extra Aharonov-Bohm phase cancels the π Berry phase and closes the gap, which is known as the wormhole effect [17–21].

The materials used to make thermoelectric generators and thermoelectric refrigerators are called thermoelectric materials, which can directly convert thermal energy into electrical energy. Thermoelectric materials have wide application prospects in thermoelectric power generation and thermoelectric refrigeration. Using thermoelectric materials to generate electricity and refrigeration will help solve the problem of energy sustainable utilization. TIs share similar material properties, such as heavy elements, narrow-band gaps, and quantum localization effect, with thermoelectric materials. Many TIs (like Bi_2Te_3, Sb_2Te_3, Bi_2Se_3, and Bi_xSb_{1-x}) are considered as excellent materials for thermoelectric conversion [22–26]. Due to the large surface-to-volume ratio and enhanced surface conductance contribution, nanoscale insulator materials bring new breakthroughs in the research of thermoelectric materials and provide new opportunities for the development of thermoelectric technology [23]. Therefore, it is very important and necessary to find high-efficiency thermoelectric materials. The conversion efficiency of thermoelectric materials depends on the dimensionless thermoelectrical figure of merit ZT. ZT is defined as $ZT = \sigma {S_c}^2 \mathcal{T}/\kappa$, where σ is the electric conductivity, S_c is the Seebeck coefficient, $\mathcal{T}$ is the operating temperature of the device, and the thermal conductivity κ is the sum of the electric thermal conductivity and lattice-thermal conductivity [22,25–29]. The higher the ZT value of the thermoelectric material, the better its performance. There are two ways to raise the ZT value. One is to increase the thermopower S_c and electrical conductivity. The larger thermopower S_c can convert the temperature difference to the voltage at both ends of the material more effectively. The other is to reduce the thermal conductivity to diminish the energy loss induced by heat diffusion and Joule heating. However, due to the restriction of the Mott relation [30] and the Wiedemann-Franz law [31], a high thermopower S_c leads to a low electrical conductance, and a high electrical conductivity also implies a high thermal conductivity. These three parameters need to be optimized to

*sunqf@pku.edu.cn

maximize the ZT value. The study of thermoelectric transport characteristics would be helpful in improving the conversion efficiency between the electrical energies and the thermal energies [22,25–27,29].

Generally, we consider the thermoelectric power, also called the Seebeck coefficient, which measures the magnitude of the longitudinal current induced by a longitudinal thermal gradient in the Seebeck effect. The thermoelectric power derived from the balance between the electric and thermal forces acting on the charge carrier is more sensitive to the details of the density of states than the electronic conductance [28,30,32–35]. Therefore, the thermoelectric power is more helpful to understand the particle-hole asymmetry of TIs. The thermoelectric power can clarify the details of the electronic structure of the ambipolar nature of the TI nanowires more clearly than the detection of conductance alone. Although the Seebeck effect and the Peltier effect provide a theoretical principle for the application of thermoelectric energy conversion and thermoelectric refrigeration [29,36], the classical Mott relation and the Wiedemann-Franz law may not be established due to the quantum behavior in nanostructured materials. Recently, Ramos-Andrade *et al.* [37] have studied the features of thermoelectric transport through a one-dimensional topological system model with Majorana bound states. It is found that there is a significant violation of Wiedemann-Franz law. Smirnov [38] also proposed that the Majorana thermoelectric signatures in nanoscopic systems such as quantum dots may be detected by using noise of the thermoelectric transport beyond linear response (see also Ref. [39]). In addition, Titvinidze *et al.* [40] have found that strong correlations can increase the thermopower of the device, by studying the influence of strong electronic interactions on the thermoelectric properties of a simple universal system. Therefore, the study of thermoelectric power may inspire new ideas in the design of quantum thermoelectric devices [40,41].

In 1993, Hicks and Dresselhaus [42] found that ZT value increases swiftly as the dimensions decrease and strongly depends on the wire width. Hicks and Dresselhaus proposed the idea of using low-dimensional structural materials to obtain high ZT. Then more and more research groups began to pay attention to the thermoelectric transport properties in nanostructure materials [43–54]. Especially in recent years, with the development of low-temperature measurement technology and the improvement of microfabrication technology (such as the synthesis of high-quality nanowires [23]), thermoelectric measurement in low-dimensional samples has became feasible at low temperature, and various groups are able to fabricate nanostructures and measure thermoelectric properties at low temperature [43,47,50–52]. In addition, the charge-carrier density in nanostructured materials can easily be tuned globally or locally by varying the magnetic field or the applied gate voltage. Due to the thermoelectric effect being sensitive to the changes of carrier density, the S_c and ZT of thermoelectric materials can be controlled by applying the magnetic field in different directions and changing the gate voltage, which opens up a broad way to find high-efficiency thermoelectric materials [27].

In this paper, we carry out a theoretical study of the thermoelectric properties of 3D TI nanowires under longitudinal and perpendicular magnetic fields by using the Landauer-Büttiker formula combined with the nonequilibrium Green's-function method. While the Fermi energy just crosses discrete transverse channels, the transmission coefficient of the quantized plateaus jumps from one step to another and the Seebeck coefficient S_c and the thermoelectric figure of merit ZT show peaks. Due to the electron-hole symmetry, S_c is an odd function of the Fermi energy E_F, and ZT is an even function. S_c and ZT have very large peaks near the Dirac point at zero magnetic field and zero gate voltage, because of the extra π Berry phase around the TI nanowire and a gap appearance in the energy spectrum. The thermoelectric properties of the TI nanowire are obviously dependent on the gate voltage and the longitudinal and perpendicular magnetic fields. The values of S_c and ZT can be easily controlled by changing the gate voltage or magnetic fields. In addition, the effect of the disorder on the thermoelectric properties is also studied. The Seebeck coefficient S_c and ZT are robust against the disorder, but the plateaus in the conductance are broken. This is very counterintuitive. Usually, the S_c and ZT are more sensitive than the conductance. In particular, the large peak value of ZT can well survive, which is very promising for the application of the thermoelectricity.

The rest of the paper is organized as follows. In Sec. II, the effective tight-binding Hamiltonian is introduced. The formalisms for calculating the Seebeck coefficient S_c and the thermoelectric figure of merit ZT are then derived. In Sec. III, the thermoelectric properties at zero perpendicular magnetic field and zero gate voltage are studied. Sections IV and V examine the effect of the perpendicular magnetic field, gate voltage, and disorder on thermoelectric properties. Finally, a brief summary is drawn in Sec. VI.

II. MODEL AND METHODS

Here we consider a cuboid 3D TI nanowire under the longitudinal and perpendicular magnetic fields as shown in Fig. 1(a). Based on the lattice model, the two-dimensional Hamiltonian for surface states of the 3D TI nanowire can be described as follows [55]:

$$H = \sum_m \Bigg[\sum_n^N c_{nm}^\dagger R_0 c_{nm} + \sum_n^N c_{nm}^\dagger R_y c_{n,m+1} + \sum_n^{N-1} c_{nm}^\dagger R_{xn} c_{n+1,m} - c_{Nm}^\dagger R_{xN} c_{1m} + \text{H.c.} \Bigg], \quad (1)$$

with

$$\begin{aligned} R_0 &= (2W/a)\sigma_z + U_n\sigma_0, \\ R_{xn} &= [-(W/2a)\sigma_z + (i\hbar v_F/2a)\sigma_y] e^{i(\phi^{\parallel}_{n,n+1} + \phi^{\perp}_{n,n+1})}, \\ R_y &= -(W/2a)\sigma_z - (i\hbar v_F/2a)\sigma_x, \end{aligned} \quad (2)$$

where c_{nm} and $c_{nm}^\dagger$ are the annihilation and creation operators at site (n,m), respectively, with the index m being along the y direction and n being along the perimeter of the TI nanowire in the xz plane. N is the total number of lattices encircling the TI nanowire; a is the lattice constant; v_F is the Fermi velocity; σ_x,σ_y, and σ_z are the Pauli matrices; σ_0 is the unit matrix; and U_n is the on-site energy which can be regulated by the gate voltage. Here we set $U_n = \Delta U/2$ for the upper surface, we set $U_n = -\Delta U/2$ for the lower

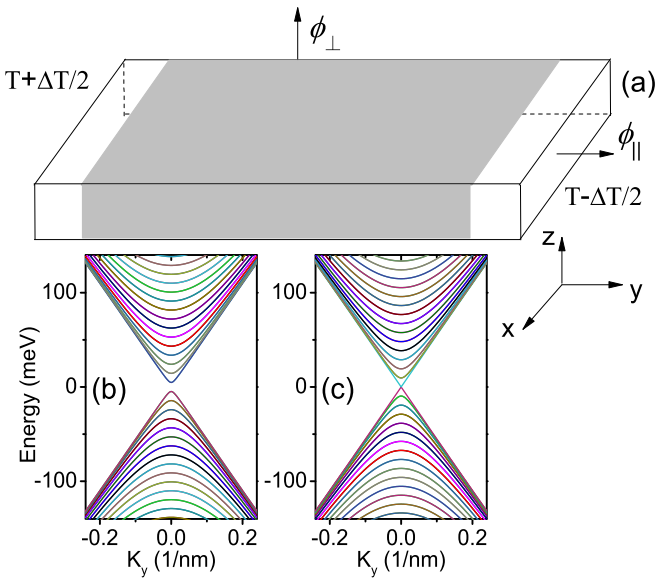

FIG. 1. (a) The schematic of a cuboid 3D TI nanowire under the longitudinal and perpendicular magnetic fields. The gray region is the center scattering region. Panels (b) and (c) show the energy-band structure of the TI nanowire with the longitudinal magnetic flux $\phi_\parallel = 0$ and π, respectively. The perpendicular magnetic field $\phi_\perp = 0$, gate voltage $\Delta U = 0$, and the disorder strength $D = 0$.

surface, and U_n is linear from $\Delta U/2$ to $-\Delta U/2$ for two side surfaces. The effect of longitudinal magnetic field is included by adding a phase term $\phi^{\parallel}_{n,n+1} = \int_n^{n+1} \mathbf{A}_\parallel \cdot d\mathbf{l}/\phi_0$ to R_{xn} in Eq. (2), where $\mathbf{A}_\parallel = (0,0,B_\parallel x)$ is the vector potential for a magnetic field $B_\parallel$ parallel to the y direction. Furthermore, we also consider a uniform magnetic field $B_\perp$ perpendicular to the upper and lower surfaces [see Fig. 1(a)]; then a phase $\phi^{\perp}_{n,n+1} = \int_n^{n+1} \mathbf{A}_\perp \cdot d\mathbf{l}/\phi_0$ is added in the hopping term R_{xn}, where $\mathbf{A}_\perp = (B_\perp y,0,0)$. W in Eq. (2) is the Wilson term. The Wilson term is introduced for solving the fermion doubling problem in the lattice model [55]. In Hamiltonian (1), the electron-electron Coulomb interaction has been ignored. Because of that the surface states are extended in two dimensions, leading the Coulomb interaction to be usually very weak. In the numerical calculations, W is set as $0.3\hbar v_F$. The nanowire is assumed to have a cross section of size $(L_x, L_z) = (96\text{ nm}, 12\text{ nm})$. For the nanowires of other sizes, the results are similar. We also set the Fermi velocity $v_F = 5\times10^5$ m/s and the lattice constant $a = 0.6$ nm [12,56].

Considering that the bias and temperature of the left and right terminal are $V_{L/R}$ and $\mathcal{T}_{L/R}$, the electronic current and the electric-thermal current flowing from the left terminal to the cuboid 3D TI nanowire can be calculated from the Landauer-Büttiker formula [29]

$$J_L = \frac{e}{h}\int T_{\mathrm{LR}}(E)[f_{\mathrm{L}}(E) - f_{\mathrm{R}}(E)]dE,$$
$$Q_L = \frac{1}{h}\int (E-\mu_L)T_{\mathrm{LR}}(E)[f_{\mathrm{L}}(E) - f_{\mathrm{R}}(E)]dE, \quad (3)$$

where the integral of energy E is from $-\infty$ to ∞. Here, we neglect the heat current carried by the phonons, because this part of the heat current is usually much smaller than that induced by the electron at low temperature. In Eq. (3),

$$f_\alpha(E,\mu_\alpha,\mathcal{T}_\alpha) = \frac{1}{e^{(E-\mu_\alpha)/k_B\mathcal{T}_\alpha}+1} \quad (4)$$

is the Fermi distribution function of the left and right terminals, where $\alpha = \mathrm{L}$ or R for the left or right terminal, and the chemical potential $\mu_\alpha = E_F + eV_\alpha$ with the Fermi energy E_F. $T_{\mathrm{LR}}(E)$ in Eq. (3) is the transmission coefficient through the 3D TI nanowire. By using the nonequilibrium Green's-function method, $T_{\mathrm{LR}}(E)$ can be obtained as $T_{\mathrm{LR}}(E) = \mathrm{Tr}[\Gamma_{\mathrm{L}}\mathbf{G}^r\Gamma_{\mathrm{R}}\mathbf{G}^a]$, in which $\Gamma_{\mathrm{L/R}}(E) = i[\Sigma^r_{\mathrm{L/R}}(E) - \Sigma^a_{\mathrm{L/R}}(E)]$ and the Green's function $\mathbf{G}^r(E) = [\mathbf{G}^a]^\dagger = [E\mathbf{I} - \mathbf{H}^{\mathrm{cen}} - \sum_\alpha \Sigma^r_\alpha]^{-1}$, with $\mathbf{H}^{\mathrm{cen}}$ being the Hamiltonian of the center scattering region and the self-energy $\Sigma^{r/a}_{\mathrm{L/R}}$ stemming from coupling to the left and right lead [57,58]. For a clean TI nanowire, the center scattering region can be arbitrarily chosen and the results are exactly identical. On the other hand, while in the presence of disorder [59], we consider that the disorder only exists in the center scattering region and the left and right terminals are disorder free. In the presence of disorder, the on-site energies at the center region are added with a term $D_{nm}\sigma_0$ with

$$D_{nm} = \sum_{n',m'} \tilde{D}_{n'm'}\exp\left(-\frac{r^2_{nm,n'm'}}{2\xi^2}\right). \quad (5)$$

Here $\tilde{D}_{n'm'}$ is uniformly distributed in the interval $[-D/2, D/2]$ with D being the disorder strength, $r_{nm,n'm'}$ the distance between site (n,m) and (n',m'), and ξ the parameter describing the correlation length of the disorder. In the numerical calculation, we consider the long-range disorder with $\xi = 5a$ and the disorder density 50%. With each value of disorder strength D, the transmission coefficient $T_{\mathrm{LR}}(E)$, the conductance, the Seebeck coefficient, thermal conductance, and ZT are averaged up to 40 configurations in the calculation.

In the case of very low bias and very small temperature gradient, the Fermi distribution function in Eq. (3) can be expanded linearly in terms of the Fermi energy E_F and the temperature $\mathcal{T}$ as

$$f_{\mathrm{L/R}}(E,\mu_{\mathrm{L/R}},\mathcal{T}_{\mathrm{L/R}}) = f_0 - eV_{\mathrm{L/R}}\frac{\partial f_0}{\partial E} + \Delta\mathcal{T}_{\mathrm{L/R}}\frac{\partial f_0}{\partial \mathcal{T}}, \quad (6)$$

where $\Delta\mathcal{T}_{\mathrm{L/R}} = \mathcal{T}_{\mathrm{L/R}} - \mathcal{T}$, and $f_0 = [e^{(E-E_F)/k_B\mathcal{T}}+1]^{-1}$ is the Fermi distribution function at zero thermal gradient and zero bias. Then linear thermoelectric transport can be calculated while a small external bias voltage $\delta V = V_{\mathrm{L}} - V_{\mathrm{R}}$ or/and a small temperature gradient $\delta\mathcal{T} = \mathcal{T}_{\mathrm{L}} - \mathcal{T}_{\mathrm{R}}$ is applied between the left and right terminals.

By introducing the integrals $I_i(\mathcal{T}) = \frac{1}{h}\int dE(E-E_F)^i(-\frac{\partial f_0}{\partial E})T_{\mathrm{LR}}(E)$ $(i = 0,1,2)$, the linear-electric conductance G ($G = I_{\mathrm{L}}/\delta V$ at zero thermal gradient), the Seebeck coefficients S_c ($S_c = \delta V/\delta\mathcal{T}$ in the zero electric current I_{L} case), and electric thermal conductance κ_e ($\kappa_e = Q_{\mathrm{L}}/\delta\mathcal{T}$ at zero electric current) can be expressed in very simple forms [27,60]:

$$G = e^2 I_0(\mathcal{T}), \quad (7)$$

$$S_c = -\frac{1}{e\mathcal{T}}\frac{I_1(\mathcal{T})}{I_0(\mathcal{T})}, \quad (8)$$

$$\kappa_e = \frac{1}{\mathcal{T}}\left[I_2(\mathcal{T}) - \frac{I_1^2(\mathcal{T})}{I_0(\mathcal{T})}\right]. \quad (9)$$

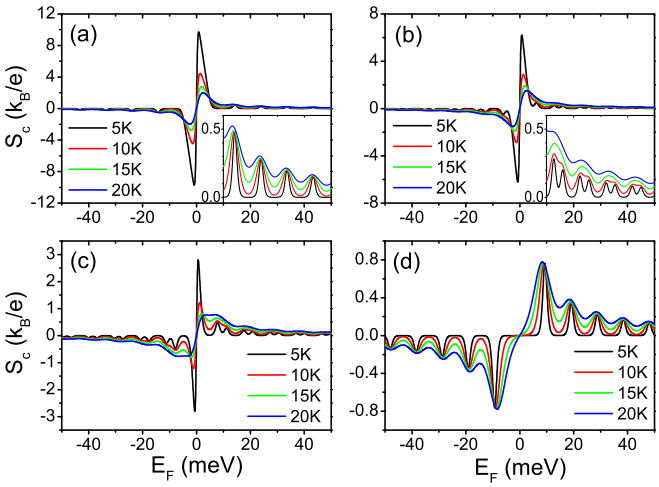

FIG. 2. Panels (a)–(d) plot the Seebeck coefficients S_c vs Fermi energy E_F for different temperatures with the longitudinal magnetic flux $\phi_\parallel = 0$, $\pi/3$, $2\pi/3$, and π, respectively. The insets in panels (a) and (b) are zoom-in figures of the small peaks in the corresponding main figures. The perpendicular magnetic field $\phi_\perp = 0$ and gate voltage $\Delta U = 0$.

After solving G, S_c, and κ_e, the thermoelectric figure of merit $ZT = GS_c{}^2\mathcal{T}/\kappa_e$ can be obtained straightforwardly.

III. THERMOELECTRIC PROPERTIES AT ZERO PERPENDICULAR MAGNETIC FIELD AND ZERO GATE VOLTAGE

First, we study the Seebeck coefficient S_c and the thermoelectric figure of merit ZT at the zero magnetic field and zero gate voltage. Figures 2(a) and 3(a) show S_c and ZT versus the Fermi energy E_F for different temperatures. Due to electron-hole symmetry, S_c is an odd function of the Fermi energy E_F with $S_c(-E_F) = -S_c(E_F)$. However, ZT is an even function of E_F with $ZT(-E_F) = ZT(E_F)$. The properties $S_c(-E_F) = -S_c(E_F)$ and $ZT(-E_F) = ZT(E_F)$ can maintain even in the presence of the magnetic field, gate voltage, and disorder. S_c and ZT exhibit a series of peaks at low temperatures. When E_F crosses the discrete transverse channels where the transmission coefficient $T_{\rm LR}$ jumps from one integer to another, S_c and ZT show peaks, which is similar to the thermopower of the quantum point contacts [61,62]. The closer the Dirac point is, the higher the peak is. S_c and ZT have the highest peak near the Dirac point. The value of ZT at the highest peak exceeds 100 at the temperature $\mathcal{T} = 10$ K. The highest peak is much higher than other peaks. For S_c (ZT), the highest peak is about 10 (100) times higher than the second highest peak. This is because of the π Berry phase around the 3D TI nanowire and the wormhole effect, and an energy gap opens at zero magnetic field at the Dirac point, implying that the transmission coefficient $T_{\rm LR} = 0$. In order to balance the thermal forces acting on the charge carriers, a very large bias is needed, which results in a very large S_c and ZT near the Dirac point. When the temperature rises, the height of the highest peak of S_c decreases, but the heights of the other peaks roughly remain unchanged and the valleys rise.

Next, we study the effect of the longitudinal magnetic field $B_\parallel$ on the Seebeck coefficient S_c and the thermoelectric figure of merit ZT. The longitudinal magnetic field is described by the magnetic flux $\Phi_\parallel$ in the cross section of the TI nanowire, with $\Phi_\parallel = L_x L_y B_\parallel$. Figures 1(b) and 1(c) show the energy-band structures of the TI nanowire at $\phi_\parallel \equiv \Phi_\parallel/\phi_0 = 0$ and π. Because of a π Berry phase for the electron going around the four facets of the TI nanowire [14–16], it yields a gapped spectrum of the surface state at $\phi_\parallel = 0$. At $\phi_\parallel = 0$, each band is doubly degenerate. With the increase of $\phi_\parallel$ from zero, the Aharonov-Bohm phase emerges and the double degeneracy is removed [19–21]. One sub-band moves up and the other sub-band goes down, implying that the gap becomes narrower. When the magnetic flux $\phi_\parallel = \pi$, the π Aharonov-Bohm phase exactly cancels the π Berry phase, implying that a pair of nondegenerate linear modes emerges with the gap closing [Fig. 1(c)]. But other bands are doubly degenerate again. Now we study the effect of the longitudinal magnetic field $\phi_\parallel$ on the thermoelectric properties. S_c and ZT are the periodic functions of $\phi_\parallel$ with $S_c(\phi_\parallel) = S_c(\phi_\parallel + 2\pi)$ and $ZT(\phi_\parallel) = ZT(\phi_\parallel + 2\pi)$. In addition, $S_c(\phi_\parallel) = S_c(-\phi_\parallel)$ and $ZT(\phi_\parallel) = ZT(-\phi_\parallel)$ because the system is invariant by simultaneously making the time-inversion transformation and rotation 180° by fixing the x axis. In Figs. 2 and 3, we show the Seebeck coefficient S_c and the thermoelectric figure of merit ZT for the longitudinal magnetic flux $\phi_\parallel = 0$, $\pi/3$, $2\pi/3$, and π, respectively. When $\phi_\parallel$ increases from zero, all peaks in the curves of $S_c \sim E_F$ and $ZT \sim E_F$ split into two due to the double degeneracy being removed. The height of the highest peak near the Dirac point also gradually decreases. Especially for ZT, the trend of decreasing is very obvious. But the value ZT is still over 30 at $\phi_\parallel = \pi/3$. For $\phi_\parallel = \pi$, the highest peak near the Dirac point completely disappears because of the close of the energy gap. But other peaks can remain the same, and the two adjacent peaks combine into a single peak again. In this case, S_c and ZT are small. Therefore, the thermoelectric properties (S_c and ZT) can be well adjusted by the longitudinal magnetic field. In fact, for $\phi_\parallel = \pi$, the magnetic field $B_\parallel$ is about 11.3 T.

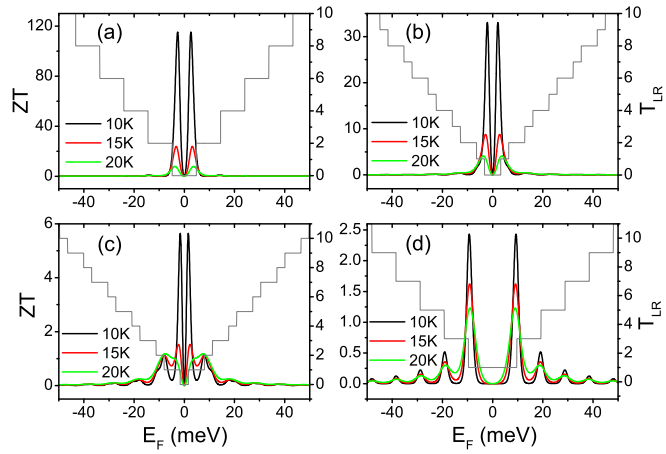

FIG. 3. Panels (a)–(d) plot ZT vs E_F for different temperatures with the longitudinal magnetic flux $\phi_\parallel = 0$, $\pi/3$, $2\pi/3$, and π, respectively. The perpendicular magnetic field $\phi_\perp = 0$ and gate voltage $\Delta U = 0$. The gray curves in panels (a)–(d) are the transmission coefficient $T_{\rm LR}$.

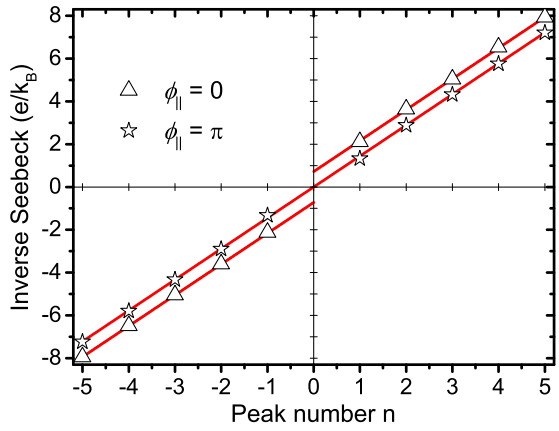

FIG. 4. The inverse of peak height of the Seebeck coefficients S_c vs the peak number n. The upper triangle symbol and hollow pentagram symbol denote the magnetic flux $\phi_\parallel = 0$ and π. These data points are obtained from the curve of $\mathcal{T} = 5$ K in Figs. 2(a) and 2(d). The two red lines are $\frac{e}{k_B}[n + \text{sign}(n)/2]/\ln 2$ and $\frac{e}{k_B} n/\ln 2$.

Figure 4 shows the inverse of the peak height of Seebeck coefficient S_c versus the peak number n with the longitudinal magnetic flux $\phi_\parallel = 0$ and π. Here the peak number n denotes the nth peak near the Dirac point, but the highest peak does not count at $\phi_\parallel = 0$. In fact, except for the highest peak, the heights of the other peaks are almost independent of temperature [see Figs. 2(a) and 2(d)]. We can see that at $\phi_\parallel = 0$ the inverse of the peak height is proportional to $\frac{e}{k_B}[n + \text{sign}(n)/2]/\ln 2$ with $\text{sign}(n) = 1$ for $n > 0$ and -1 for $n < 0$ (see the upper triangle symbol in Fig. 4). This is similar to that in the conventional metal [28]. On the other hand, for $\phi_\parallel = \pi$, the inverse of the peak height is proportional to $\frac{e}{k_B} n/\ln 2$ (see the hollow pentagram symbol in Fig. 4), which is similar to that in graphene [28]. This is because the extra π Berry phase and the wormhole effect lead to a half-integer shift in the curve of the inverse of the peak height of S_c versus the peak number n. In fact, these conclusions can also be analytically obtained from the energy-band structure and the transmission coefficient $T_{\text{LR}}(E)$. Taking $\phi_\parallel = 0$ with positive n as an example, when the energy E is in the vicinity of E_n, the transmission coefficient $T_{\text{LR}}(E)$ can be written as $T_{\text{LR}}(E) = 2n$ at $E < E_n$ and it jumps to $2n + 2$ at $E > E_n$ with E_n being the bottom of the nth sub-band. Then substituting this transmission coefficient $T_{\text{LR}}(E)$ into Eq. (8), we can obtain

$$S_c(E_F) = \frac{k_B}{e} \frac{-xe^x + (1 + e^x)\ln(1 + e^x)}{1 + n(1 + e^x)}, \tag{10}$$

with $x \equiv (E_n - E_F)/k_B\text{T}$. This equation gives the shape of the nth peak for $\phi_\parallel = 0$ with positive n. So the height of the nth peak of S_c is about $\frac{k_B}{e}\ln 2/(n + 1/2)$. From $S_c(-E_F) = -S_c(E_F)$, the peak heights for negative n can be obtained as $\frac{k_B}{e}\ln 2/(n - 1/2)$ straightforwardly. Similarly, the shape of the nth peak of S_c for $\phi_\parallel = \pi$ can analytically be derived as

$$S_c(E_F) = \frac{k_B}{e} \frac{-xe^x + (1 + e^x)\ln(1 + e^x)}{1 + (n - 1/2)(1 + e^x)}, \tag{11}$$

and the peak height is $\frac{k_B}{e}\ln 2/n$. In Fig. 4, the curves $\frac{e}{k_B}[n + \text{sign}(n)/2]/\ln 2$ and $\frac{e}{k_B} n/\ln 2$ (the analytic results for the inverse of the peak height of S_c) are also shown. They are well consistent with the numerical points.

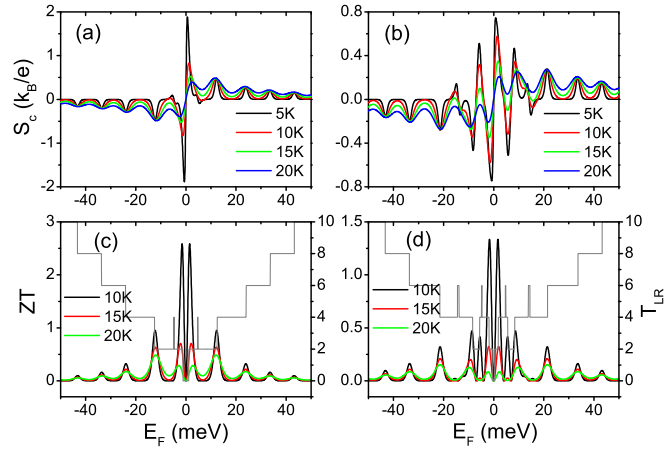

FIG. 5. The Seebeck coefficient S_c and ZT vs Fermi energy E_F for different temperatures. $\phi_\parallel = 0$, $\phi_\perp = 0$, and the gate voltage $\Delta U = 30$ meV in panels (a) and (c) and $\Delta U = 50$ meV in panels (b) and (d). The gray curves in panels (c) and (d) are the transmission coefficient T_{LR}.

IV. EFFECT OF THE PERPENDICULAR MAGNETIC FIELD AND GATE VOLTAGE ON THERMOELECTRIC PROPERTIES

In this section, we study the effect of the perpendicular magnetic field $B_\perp$ and gate voltage ΔU on the Seebeck coefficient S_c and thermoelectrical figure of merit ZT of the 3D TI nanowire. First, the effect of ΔU is studied. Figure 5 shows S_c and ZT with $\phi_\parallel = 0$, and the gate voltage ΔU being 30 and 50 meV. The parameters in Fig. 6 are similar to those in Fig. 5, but $\phi_\parallel = \pi$. In order to explain the behavior of S_c and ZT clearly, the transmission coefficient T_{LR} is also given in Figs. 5 and 6, and here T_{LR} is quantized and exhibits a series of plateaus. In Fig. 5, when T_{LR} jumps from one step to another, we see that S_c and ZT show peaks at the longitudinal magnetic flux $\phi_\parallel = 0$. In particular, as the gate

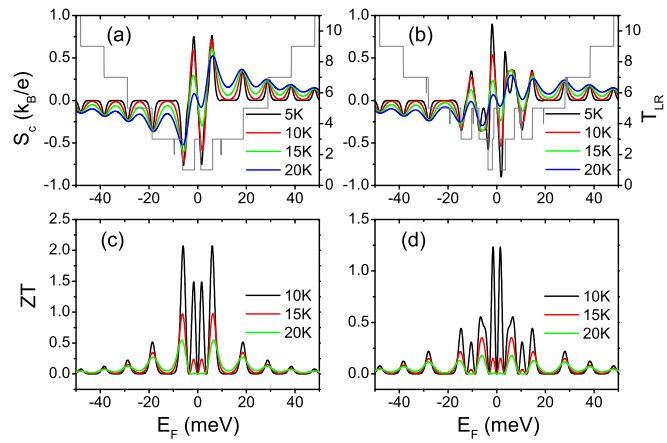

FIG. 6. S_c and ZT vs Fermi energy E_F for different temperatures. $\phi_\parallel = \pi$, $\phi_\perp = 0$, and the gate voltage $\Delta U = 30$ meV in panels (a) and (c) and $\Delta U = 50$ meV in panels (b) and (d). The gray curves in panels (a) and (b) are the transmission coefficient T_{LR}.

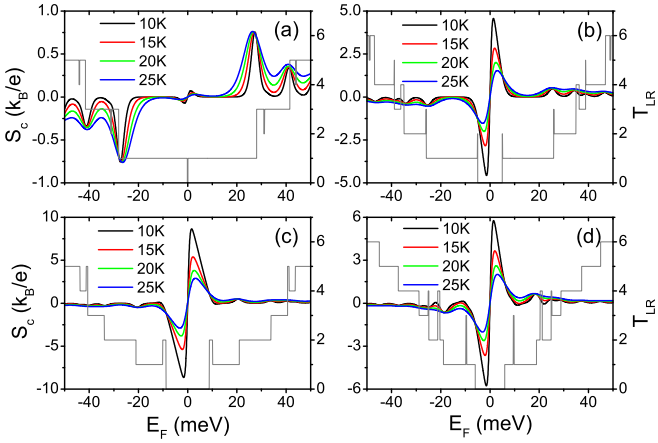

FIG. 7. The Seebeck coefficient S_c vs E_F for different temperatures with the perpendicular magnetic field $\phi_\perp = 0.005$ and $\phi_\parallel = 0$. The gate voltage $\Delta U = 0$ meV (a), 10 meV (b), 20 meV (c), and 50 meV (d). The gray curves in panels (a)–(d) are the transmission coefficient $T_{\rm LR}$.

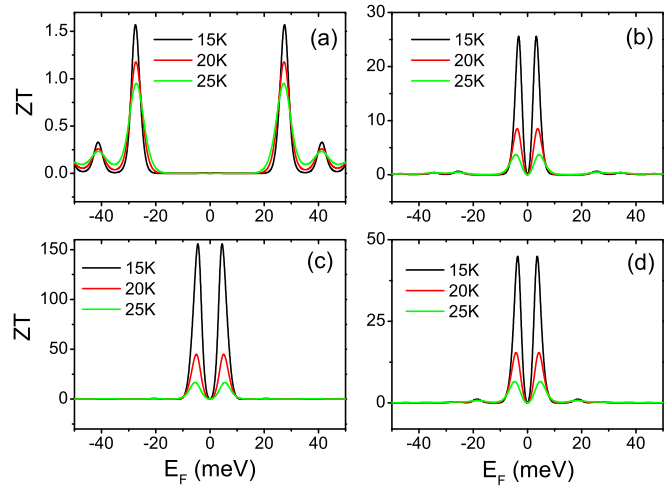

FIG. 8. ZT vs E_F for different temperatures with $\phi_\perp = 0.005$ and $\phi_\parallel = 0$. The gate voltage $\Delta U = 0$ meV (a), 10 meV (b), 20 meV (c), and 50 meV (d).

voltage increases, the large ZT at $\Delta U = 0$ [see Fig. 3(a)] reduces swiftly. When $\Delta U = 20$ meV, the value of ZT is about 15.6. So the gate voltage can regulate the thermoelectric properties. In addition, the oscillation peaks near the Dirac point become dense in the presence of ΔU [see Figs. 5(b) and 5(d)]. Because the gate voltage ΔU causes the difference between the potential energies of the upper and lower surfaces, ΔU affects the states of the side surfaces, and makes the energy band deform, which leads to a strong reduction of the energy gap. Figure 6 shows the curve of $S_c \sim E_F$ and $ZT \sim E_F$ at the longitudinal magnetic flux $\phi_\parallel = \pi$. Similarly, S_c and ZT display peaks when the transmission coefficient $T_{\rm LR}$ step jumps. The dense peaks exhibit near the Dirac point when the gate voltage ΔU increases. By comparing between Figs. 5(b) and 5(d) and Figs. 6(b) and 6(d) for $\Delta U = 50$ meV, we find that the curves of $S_c \sim E_F$ and $ZT \sim E_F$ are very similar, although $\phi_\parallel = 0$ in Fig. 5 and $\phi_\parallel = \pi$ in Fig. 6. This means that both the π Berry phase and the Aharonov-Bohm phase of $\phi_\parallel$ have little effect on the Seebeck coefficient S_c and ZT while at the large gate voltage.

Now, we study the effect of the perpendicular magnetic field $B_\perp$ on the Seebeck coefficient S_c and the thermoelectric figure of merit ZT. For small $B_\perp$ (e.g., $B_\perp < 0.1$ T), S_c and ZT are almost unaffected, and ZT still has a large value at $\phi_\parallel = 0$. On the other hand, for a large perpendicular magnetic field $B_\perp$, Landau levels form and edge states appear on the side surfaces. In this case, S_c and ZT are almost independent of the longitudinal magnetic field $\phi_\parallel$ and ZT strongly reduces. Figures 7(a) and 8(a) show S_c and ZT versus the Fermi energy E_F with the perpendicular magnetic flux in a lattice $\phi_\perp = 0.005$ (the real magnetic field $B_\perp$ is around 18.3 T). S_c displays peaks when E_F passes the Landau levels. Meanwhile, S_c shows valleys between adjacent Landau levels. Because the Landau levels are highly degenerate, the number of energy levels decreases. As a result the peak spacing becomes larger and the peak becomes sparse. When E_F is on the zeroth Landau level, S_c is zero. This is because the zeroth Landau level with double degeneracy is shared equally by electrons and holes, and the electrons and holes give the opposite contributions to S_c. Moreover, the peak height of S_c is proportional to $\frac{k_B}{e}\ln 2/n$ with n being the peak number. With the increase of temperature $\mathcal{T}$, the peak height of S_c remains approximately unchanged, but the valley rises, which shows that S_c peaks are robust against the temperature. For the thermoelectric figure of merit ZT, it is small for all the Fermi energy E_F, because of the appearance of the edge states and the absence of the energy gap at large $\phi_\perp$. In addition, the two largest peaks in ZT are at $E_F \approx \pm 27.3$ meV (27.3 meV is the first Landau level). The positions of the ZT peaks are corresponding to the S_c peaks. With the increase of $\phi_\perp$, the peak spacing of ZT becomes larger and the peak becomes sparse similar to the peaks of S_c.

Let us study the case of the coexistence of both the perpendicular magnetic field $\phi_\perp$ and gate voltage ΔU. Figures 7(b)–7(d) and 8(b)–8(d) show S_c and ZT at large $\phi_\perp$ ($\phi_\perp = 0.005$) and zero $\phi_\parallel$ for the different ΔU. For large $\phi_\perp$, Landau levels form, and both S_c and ZT are almost independent of the longitudinal magnetic flux $\phi_\parallel$. When the gate voltage ΔU is applied, the Landau levels of the upper and lower surfaces split, which produces a gap spectrum of surface states in the TI nanowire. So the highest peaks of S_c and ZT near the Dirac point appear, and the value of ZT strongly increases. While $\Delta U \geqslant 10$ meV, ZT can exceed 25. In addition, we can see from Figs. 7 and 8 that, when the gate voltage increases, the band gap of surface states increases first and then decreases due to the side surfaces. So the highest peak of S_c and ZT also tends to increase first and then decreases. But ZT can remain a large value in a very large range of ΔU. In short, by adjusting the longitudinal and perpendicular magnetic fields and the gate voltage, it is easy to change the value of S_c and ZT greatly, i.e., to change greatly the thermoelectric properties of the 3D TI nanowire.

V. EFFECT OF DISORDER ON THERMOELECTRIC PROPERTIES

Up to now, we have shown that the Seebeck coefficient S_c and the thermoelectric figure of merit ZT have large value

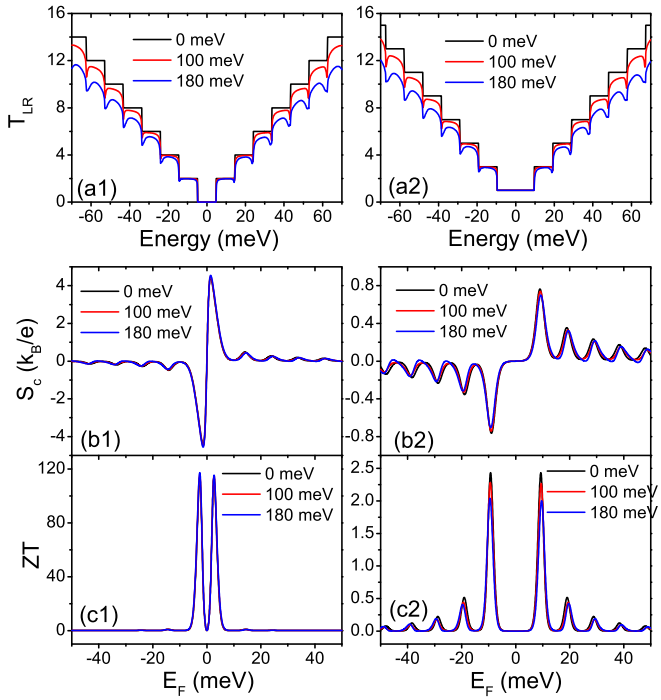

FIG. 9. The transmission coefficient $T_{\rm LR}$ vs the energy E (a), the Seebeck coefficient S_c vs E_F (b), and ZT vs E_F (c) for the different disorder strength D. The temperature $\mathcal{T} = 10$ K, the gate voltage $\Delta U = 0$ meV, $\phi_\perp = 0$, and $\phi_\parallel = 0$ for panels (a1)–(c1) and π for panels (a2)–(c2).

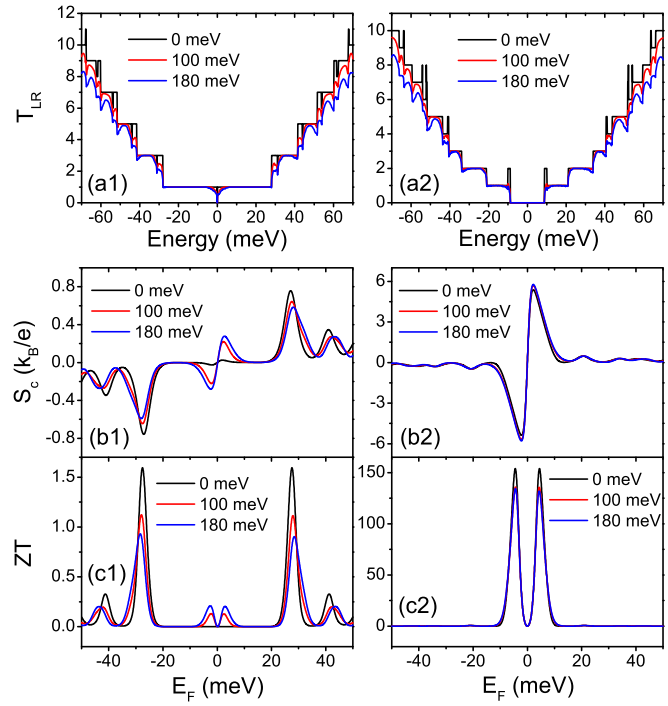

FIG. 10. $T_{\rm LR}$ vs energy E (a), S_c vs E_F (b), and ZT vs E_F (c) for the different disorder strength D. The perpendicular magnetic field $\phi_\perp = 0.005$, the longitudinal magnetic field $\phi_\parallel = 0$, the temperature $\mathcal{T} = 15$ K, and the gate voltage $\Delta U = 0$ meV for the panels (a1)–(c1) and 20 meV for the panels (a2)–(c2).

at zero magnetic fields with zero gate voltage, or at large perpendicular magnetic field with nonzero gate voltage. Next, let us study the effect of disorder on S_c and ZT. Figure 9 shows the transmission coefficient $T_{\rm LR}$, S_c, and ZT for the different disorder strengths D at zero perpendicular magnetic field. When the disorder strength $D = 0$, $T_{\rm LR}$ displays quantum plateaus. While in the presence of disorder ($D \neq 0$), the lower plateaus (e.g., the plateaus with $T_{\rm LR} = 0$ and 1) are robust against disorder. On the other hand, the higher plateaus of $T_{\rm LR}$ are obviously destroyed, because the scattering occurs by disorder. But the results show that S_c and ZT are very robust against disorder in a wide range of Fermi energy E_F. Not only can the highest peak near the Dirac point survive, but also the low peaks at large E_F can remain at strong disorder. Even if the disorder strength $D = 180$ meV, the peak value of ZT can still exceed 100 [see Fig. 9(c1)] and these lower peaks remain almost the same [see Figs. 9(b1), 9(b2), and 9(c2)]. This is obviously counterintuitive, because thermoelectric behaviors (S_c and ZT) are more sensitive to the density of states than the conductance (or transmission coefficient). In fact, although the plateaus of $T_{\rm LR}$ are obviously destroyed by disorder, the sudden jumps from one plateau to another still exist and the position of the jump point remains unchanged. Because the peaks of S_c and ZT are mainly determined by the jumps of $T_{\rm LR}$, they are robust against disorder. ZT is robust against disorder and has a large value. These characteristics of ZT are very helpful for the application of thermoelectricity.

Figure 10 shows the transmission coefficient $T_{\rm LR}$, S_c, and ZT for the different disorder strengths at the high perpendicular magnetic field $\phi_\perp = 0.005$ with the gate voltage $\Delta U = 0$ and 20 meV. While $\Delta U = 0$, S_c and ZT are small for the clean TI nanowire. The disorder reduces the heights of the peaks of S_c and ZT, and slightly shifts the peak positions as well. For example, while the disorder strength $D = 180$ meV, the peak heights of ZT decrease to about half of that at $D = 0$. On the other hand, for the case with nonzero gate voltage (e.g., $\Delta U = 20$ meV), S_c and ZT have large peak values while the disorder strength $D = 0$. With the increase of D, the peak heights and positions of S_c and ZT can remain almost unchanged. When $D = 180$ meV, the largest value of ZT can still exceed 100. ZT not only has a large value but also is robust against disorder, which is very promising for application.

VI. CONCLUSIONS

In summary, we study the magnetothermoelectric transport properties of the surface states of 3D TI nanowires under longitudinal and perpendicular magnetic fields. The Seebeck coefficient S_c and the thermoelectric figure of merit ZT show peaks where there are step changes of the transmission coefficient. Due to electron-hole symmetry, the Seebeck coefficient is an odd function of the Fermi energy E_F, and ZT is an even function. The highest peak appears when E_F is near the Dirac point, and the peak heights gradually decrease with E_F far from the Dirac point. At zero magnetic field and zero gate voltage, the Seebeck coefficient S_c and ZT have large peak value due to the π Berry phase around the topological insulator nanowire and the wormhole effect. The Seebeck coefficient S_c and ZT are obviously dependent on the gate voltage and the longitudinal and perpendicular magnetic fields.

This means that the thermoelectric properties of the 3D TI nanowire can be easily adjusted by tuning the gate voltage or magnetic fields. At zero magnetic field and zero gate voltage, or at large perpendicular magnetic field and nonzero gate voltage, ZT has a large value. In addition, the effect of disorder on the thermoelectric properties is also studied. It is a surprise that the Seebeck coefficient and ZT are more undisturbed than the conductance (transmission coefficient). The plateaus of the transmission coefficient can be broken by disorder, but the peaks of the Seebeck coefficient and ZT are robust against disorder, because the jumps of the transmission coefficient can remain in the presence of disorder. The characteristics, that ZT has a large value and is robust against disorder, are very beneficial for the application of thermoelectricity.

ACKNOWLEDGMENTS

This paper was financially supported by the National Key Research and Development Program of China (Grant No. 2017YFA0303301), the National Basic Research Program of China (Grant No. 2015CB921102), the National Natural Science Foundation of China (Grant No. 11574007), and the Key Research Program of the Chinese Academy of Sciences (Grant No. XDPB08-4).

[1] C. L. Kane and E. J. Mele, Phys. Rev. Lett. **95**, 226801 (2005).
[2] B. A. Bernevig, T. L. Hughes, and S.-C. Zhang, Science **314**, 1757 (2006).
[3] M. König, S. Wiedmann, C. Brüne, A. Roth, H. Buhmann, L. W. Molenkamp, X.-L. Qi, and S.-C. Zhang, Science **318**, 766 (2007).
[4] M. Z. Hasan and C. L. Kane, Rev. Mod. Phys. **82**, 3045 (2010).
[5] X.-L. Qi and S.-C. Zhang, Rev. Mod. Phys. **83**, 1057 (2011).
[6] H. Zhang, C.-X. Liu, X.-L. Qi, X. Dai, Z. Fang, and S.-C. Zhang, Nat. Phys. **5**, 438 (2009).
[7] Y. L. Chen, J. G. Analytis, J.-H. Chu, Z. K. Liu, S.-K. Mo, X. L. Qi, H. J. Zhang, D. H. Lu, X. Dai, Z. Fang, S. C. Zhang, I. R. Fisher, Z. Hussain, and Z.-X. Shen, Science **325**, 178 (2009).
[8] Y. Xia, D. Qian, D. Hsieh, L. Wray, A. Pal, H. Lin, A. Bansil, D. Grauer, Y. S. Hor, R. J. Cava, and M. Z. Hasan, Nat. Phys. **5**, 398 (2009).
[9] H. Jiang, S. Cheng, Q.-F. Sun, and X. C. Xie, Phys. Rev. Lett. **103**, 036803 (2009).
[10] D. Hsieh, Y. Xia, L. Wray, D. Qian, A. Pal, J. H. Dil, J. Osterwalder, F. Meier, G. Bihlmayer, C. L. Kane, Y. S. Hor, R. J. Cava, and M. Z. Hasan, Science **323**, 919 (2009).
[11] Y. Xu, I. Miotkowski, C. Liu, J. Tian, H. Nam, N. Alidoust, J. Hu, C.-K. Shih, M. Z. Hasan, and Y. P. Chen, Nat. Phys. **10**, 956 (2014); Y. Xu, I. Miotkowski, and Y. P. Chen, Nat. Commun. **7**, 11434 (2016).
[12] R. Yoshimi, A. Tsukazaki, Y. Kozuka, J. Falson, K. S. Takahashi, J. G. Checkelsky, N. Nagaosa, M. Kawasaki, and Y. Tokura, Nat. Commun. **6**, 6627 (2015).
[13] N. Koirala, M. Brahlek, M. Salehi, L. Wu, J. Dai, J. Waugh, T. Nummy, M.-G. Han, J. Moon, Y. Zhu, D. Dessau, W. Wu, N. P. Armitage, and S. Oh, Nano Lett. **15**, 8245 (2015).
[14] J. H. Bardarson, P. W. Brouwer, and J. E. Moore, Phys. Rev. Lett. **105**, 156803 (2010).
[15] R. Egger, A. Zazunov, and A. L. Yeyati, Phys. Rev. Lett. **105**, 136403 (2010).
[16] Y. Zhang and A. Vishwanath, Phys. Rev. Lett. **105**, 206601 (2010).
[17] H. Peng, K. Lai, D. Kong, S. Meister, Y. Chen, X.-L. Qi, S.-C. Zhang, Z.-X. Shen, and Y. Cui, Nat. Mater. **9**, 225 (2010).
[18] F. Xiu, L. He, Y. Wang, L. Cheng, L.-T. Chang, M. Lang, G. Huang, X. Kou, Y. Zhou, X. Jiang, Z. Chen, J. Zou, A. Shailos, and K. L. Wang, Nat. Nanotechnol. **6**, 216 (2011).
[19] J. Dufouleur, L. Veyrat, A. Teichgräber, S. Neuhaus, C. Nowka, S. Hampel, J. Cayssol, J. Schumann, B. Eichler, O. G. Schmidt, B. Büchner, and R. Giraud, Phys. Rev. Lett. **110**, 186806 (2013).
[20] S. S. Hong, Y. Zhang, J. J. Cha, X.-L. Qi, and Y. Cui, Nano Lett. **14**, 2815 (2014).
[21] S. Cho, B. Dellabetta, R. Zhong, J. Schneeloch, T. Liu, G. Gu, M. J. Gilbert, and N. Mason, Nat. Commun. **6**, 7634 (2015).
[22] L. Müchler, F. Casper, B. Yan, S. Chadov, and C. Felser, Phys. Status Solidi RRL **7**, 91 (2013).
[23] D. Kong, J. C Randel, H. Peng, J. J Cha, S. Meister, K. Lai, Y. Chen, Z. X Shen, H. C Manoharan, and Y. Cui, Nano Lett. **10**, 329 (2010).
[24] J. Gooth, J. G. Gluschke, R. Zierold, M. Leijnse, H. Linke, and K. Nielsch, Semicond. Sci. Technol. **30**, 015015 (2015).
[25] N. Xu, Y. Xu, and J. Zhu, npj Quantum Mater. **2**, 51 (2017).
[26] J. He and T. M. Tritt, Science **357**, eaak9997 (2017).
[27] J. Liu, Q.-F. Sun, and X. C. Xie, Phys. Rev. B **81**, 245323 (2010).
[28] Y. Xing, Q.-F. Sun, and J. Wang, Phys. Rev. B **80**, 235411 (2009).
[29] M. M. Wei, Y. T. Zhang, A. M. Guo, J. J Liu, Y. Xing, and Q.-F. Sun, Phys. Rev. B **93**, 245432 (2016).
[30] M. Cutler and N. F. Mott, Phys. Rev. **181**, 1336 (1969).
[31] G. Jeffrey Snyder and E. S. Toberer, Nat. Mater. **7**, 105 (2008).
[32] A. A. Abrikosov, *Fundamentals of the Theory of Metals* (North-Holland, Amsterdam, 1988); D. K. C. Macdonald, *Thermoelectricity* (Dover, New York, 2006).
[33] C. W. J. Beenakker and A. A. M. Staring, Phys. Rev. B **46**, 9667 (1992).
[34] S.-G. Cheng, Y. Xing, Q.-F. Sun, and X. C. Xie, Phys. Rev. B **78**, 045302 (2008).
[35] Y. Zhang, J. Song, and Y.-X. Li, J. Appl. Phys **117**, 124301 (2015).
[36] H. B. Callen, Phys. Rev. **73**, 1349 (1948); **85**, 16 (1952).
[37] J. P. Ramos-Andrade, O. Ävalos-Ovando, P. A. Orellana, and S. E. Ulloa, Phys. Rev. B **94**, 155436 (2016).
[38] S. Smirnov, Phys. Rev. B **97**, 165434 (2018).
[39] L. Fu and C. L. Kane, Phys. Rev. Lett. **100**, 096407 (2008).
[40] I. Titvinidze, A. Dorda, W.von der Linden, and E. Arrigoni, Phys. Rev. B **96**, 115104 (2017).
[41] B. Kubala, J. König, and J. Pekola, Phys. Rev. Lett. **100**, 066801 (2008).
[42] L. D. Hicks and M. S. Dresselhaus, Phys. Rev. B **47**, 16631 (1993).
[43] T. Miyasato, N. Abe, T. Fujii, A. Asamitsu, S. Onoda, Y. Onose, N. Nagaosa, and Y. Tokura, Phys. Rev. Lett. **99**, 086602 (2007).
[44] S. Onoda, N. Sugimoto, and N. Nagaosa, Phys. Rev. B **77**, 165103 (2008).
[45] R. Ma, L. Sheng, M. Liu, and D. N. Sheng, Phys. Rev. B **87**, 115304 (2013).

[46] Y. Xu, Z. Gan, and S.-C. Zhang, Phys. Rev. Lett. **112**, 226801 (2014).
[47] J. Zhang, X. Feng, Y. Xu, M. Guo, Z. Zhang, Y. Ou, Y. Feng, K. Li, H. Zhang, L. Wang, X. Chen, Z. Gan, S.-C. Zhang, K. He, X. Ma, Q.-K. Xue, and Y. Wang, Phys. Rev. B **91**, 075431 (2015).
[48] B. Z. Rameshti and R. Asgari, Phys. Rev. B **94**, 205401 (2016).
[49] J.-W. Li, B. Wang, Y.-J. Yu, Y.-D. Wei, Z.-Z. Yu, and Y. Wang, Front. Phys. **12**, 126501 (2017).
[50] S. Y. Matsushita, K. K. Huynh, H. Yoshino, N. H. Tu, Y. Tanabe, and K. Tanigaki, Phys. Rev. Mater. **1**, 054202 (2017).
[51] D. S. Shapiro, D. E. Feldman, A. D. Mirlin, and A. Shnirman, Phys. Rev. B **95**, 195425 (2017).
[52] S. I. Erlingsson, A. Manolescu, G. A. Nemnes, J. H. Bardarson, and D. Sanchez, Phys. Rev. Lett. **119**, 036804 (2017).
[53] M.-S. Lim and S.-H. Jhi, Solid State Commun. **270**, 22 (2018).
[54] A. Mani and C. Benjamin, Phys. Rev. E **96**, 032118 (2017); **97**, 022114 (2018).
[55] Y.-F. Zhou, H. Jiang, X. C. Xie, and Q.-F. Sun, Phys. Rev. B **95**, 245137 (2017).
[56] T. Zhang, P. Cheng, X. Chen, J.-F. Jia, X. Ma, K. He, L. Wang, H. Zhang, X. Dai, Z. Fang, X. Xie, and Q.-K. Xue, Phys. Rev. Lett. **103**, 266803 (2009).
[57] W. Long, Q.-F. Sun, and J. Wang, Phys. Rev. Lett. **101**, 166806 (2008).
[58] D. H. Lee and J. D. Joannopoulos, Phys. Rev. B **23**, 4997 (1981).
[59] S. Cheng, J. Zhou, H. Jiang, and Q.-F. Sun, New J. Phys. **18**, 103024 (2016).
[60] T. A. Costi and V. Zlatic, Phys. Rev. B **81**, 235127 (2010).
[61] C. R. Proetto, Phys. Rev. B **44**, 9096 (1991).
[62] H.van. Houten, L. W Molenkamp, C. W. J Beenakker, and C. T Foxon, Semicond. Sci. Technol **7**, B215 (1992).